Aerosol and Air Quality Research, 18: 15–25, 2018
Copyright © Taiwan Association for Aerosol Research
ISSN: 1680-8584 print / 2071-1409 online
doi: 10.4209/aaqr.2017.01.0029

Aqueous Secondary Organic Aerosol Formation in Ambient Cloud Water Photo-Oxidations

Misha I. Schurman[1,2*], Alexandra Boris[1], Yury Desyaterik[1], Jeffrey L. Collett, Jr.[1]

[1] *Department of Atmospheric Science, Colorado State University, Fort Collins, CO 80521, USA*
[2] *Colorado Mountain College, Breckenridge, CO 80424, USA*

ABSTRACT

The current understanding of aqueous secondary organic aerosol (aqSOA) formation is based largely on laboratory investigations of very simple surrogate cloud water solutions that aid mechanistic understanding of aqueous oxidation but may not accurately reflect the influence of the complex ambient matrix present in authentic cloud waters on organic chemistry. In this study, unaltered ambient cloud water and 'biogenically influenced' ambient cloud water (with added pinonic acid) were photo-oxidized, atomized, and dried to simulate the formation of aqSOA in clouds, then analyzed using an Aerodyne Aerosol Mass Spectrometer. Two major chemical regimes were identified: in the first, particle organic mass is gained, then lost; sustained increases in highly oxidized fragments indicate overall organic acid formation, while increases in nominally volatile fragments suggest that evaporation may contribute to the observed mass decrease. In the second regime, the oxidation level of cloud water organic matter decreases as mass decreases, suggesting that oxidized functional groups are fragmented and lost to evaporation. Overall, the rate of aqSOA production in unaltered cloud water decreases as oxygenation increases, until organic mass loss beginning at consistent values of $f44 > 0.23 \pm 0.05$ and O:C > 0.61 ± 0.05. We hypothesize that there may be a parameterizable 'maximum oxidation level' for cloud water above which functional group fragmentation is dominant. These experiments are among the first to quantify organic mass production in ambient cloud water and employ the most atmospherically relevant oxidant concentrations to date.

Keywords: Secondary organic aerosol; Cloud chemistry; Photooxidation; Aqueous.

INTRODUCTION

Particles in the atmosphere have wide-ranging health, environmental, and climate effects, many of which are attributed disproportionately to fine-mode (< 2.5 μm diameter) secondary organic aerosols (SOA). While gas-phase chemistry and subsequent partitioning was traditionally thought to be the main source of SOA, this mechanism fails to predict the amount, content (Chang and Thompson, 2010), distribution (Tsigaridis and Kanakidou, 2003; Heald *et al.*, 2005), and size of ambient particles (Blando and Turpin, 2000), where 'ambient particles' are defined as particles found in ambient air; recent work suggests that up to ~50% of total SOA mass is formed through aqueous reactions (Ervens *et al.*, 2011). However, most of our knowledge of SOA formation is based on laboratory investigations of very simple solutions that aid mechanistic understanding of aqueous oxidation but may not accurately reflect the influence of the complex ambient matrix (defined as the mixture of compounds comprising a cloud water sample) on organic chemistry (Boris *et al.*, 2014). This paper seeks to investigate the relevance of previous aqueous SOA (aqSOA) studies by photo-oxidizing ambient cloud water (defined as cloud water collected in-situ from natural clouds) with and without addition of common aqSOA precursors; while the complexity of the cloud water matrix prevents precise mechanistic determination, general reaction regimes may be inferred in terms of changes in organic mass, composition, and level of oxidation. Such an approach can be very useful, especially given our incomplete understanding of the organic composition of ambient aerosols and cloud water.

Important aqSOA precursors include anthropogenic and biogenic volatile organic compounds (A- and B-VOCs, respectively) oxidized to form products such as glyoxal, methylglyoxal, pinonaldehyde, and pinic/pinonic acids (Atkinson and Arey, 2003; Fu *et al.*, 2008). Pinonic acid is used herein to represent oxidation products of α-pinene which may be absorbed from cloud interstitial spaces (Jang, 1999; Kanakidou *et al.*, 2005), as a proxy for total interstitial BVOC absorption. We hypothesize that this addition of organic material, and its relatively low oxidation level relative

* Corresponding author.
Tel.: 1-720-485-9191
E-mail address: mishaschurman.ms@gmail.com

to the original cloudwater, may augment and/or sustain aqSOA formation as found in the previous works (see discussion in Results Section).

The hydroxyl radical (OH) is a dominant aqueous oxidant (Herrmann *et al.*, 2010). OH can be absorbed from the gas phase, but is also formed significantly (up to ~33%; Ervens *et al.*, 2003b; Arakaki and Faust, 1998) by aqueous photolysis of hydrogen peroxide (H_2O_2; Graedel and Goldberg, 1983; Zellner *et al.*, 1990), iron(III) hydroxide ($Fe(OH)^{2+}$; Weschler *et al.*, 1986; Arakaki and Faust, 1998), nitrous acid (HONO; Fischer and Warneck, 1996; Arakaki and Faust, 1998), and nitric acid (HNO_3; Graedel and Weschler, 1981); H_2O_2 and HO_x (HO+ hydroperoxyl radical, HO_2) may also undergo regenerative chemistry involving organic radicals (Anastasio *et al.*, 1994; Valverde-Canossa *et al.*, 2005). Direct organic photolytic oligomerization and lysing reactions are also possible and may form OH in turn through HO_x cycling, though organic radical-initiated reactions are generally not competitive with OH oxidation (Guzman *et al.*, 2006; Tan *et al.*, 2010; Tan *et al.*, 2012). Fenton reactions may produce OH in the absence of ultraviolet light (UV; Arakaki and Faust, 1998; Deguillaume *et al.*, 2005), which motivated our no-UV control experiments. Reaction with OH and photolysis are important aqueous pinonic acid sinks (Lignell *et al.*, 2013).

The current understanding of aqSOA mechanisms, products, and yields is based largely on laboratory investigations of simple solutions with unrealistically high oxidant and reactant concentrations. Solute concentration strongly influences aqSOA yield and product type, with higher concentrations forming higher molecular weight compounds such as oligomers through organic self-reaction, while lower fog- and cloud-relevant concentrations often form organic acids (Tan *et al.*, 2009; Lim *et al.*, 2010). Solute composition is also important, as organic radical formation, hygroscopicity, acidity, and component distribution in the droplet (e.g., organic shells) may all affect aqSOA yields (Volkamer *et al.*, 2009; Ervens and Volkamer, 2010; Galloway *et al.*, 2011).

Simple solutions of common SOA precursors, while more mechanistically constrained, may not accurately represent the complex chemistry in real atmospheric waters. This work explores how photooxidation influences ambient cloud water organic mass, average oxidation state, and reaction regimes (such as functionalization versus fragmentation), and investigates relationships between oxidative progression and solution characteristics such as total organic carbon (TOC) and oxidation level (oxygen-to-carbon elemental ratios (O:C), *f*44, etc.). The experiments presented here compare bulk photo-oxidations of real cloud water and cloud water with added pinonic acid (simulating 'biogenic precursor' addition), all featuring among the most atmospherically relevant reactant and oxidant concentrations to date.

METHODS

The Aerodyne High Resolution Time-of-Flight Aerosol Mass Spectrometer (AMS) measures the size and composition of submicron non-refractory particles with high time- and mass-resolution and has been described elsewhere (Decarlo *et al.*, 2006); vaporization and electron impact ionization therein cause molecular fragmentation, complicating identification of specific reaction products as discussed later. AMS data quality is constrained by rigorous calibration; a LI-COR LI-820 monitor before the inlet constrained $CO_{2(g)}$ contributions to the CO_2^+ fragment. The ToF-AMS DAQ v 1.7.2B software was used for data acquisition; data analysis utilized the SQUIRREL (v1.52K) and PIKA (v1.11K, Sueper *et al.*, 2011) tools in Igor Pro 6.22A (WaveMetrics Inc., Lake Oswego, OR). Measurements near the AMS detection limit were not altered or eliminated. Particulars can be found in the supplement.

Briefly, bulk solutions are oxidized in a beaker-like vessel using UV light (Green Killing Machine, Model AAUV09W-UVC, 254 nm peak wavelength) and hydrogen peroxide, atomized (TSI 3076), dried (mimicking particle formation from cloud droplet evaporation, Loeffler *et al.*, 2006; De Haan *et al.*, 2009; El Haddad *et al.*, 2009; Lee *et al.*, 2011a), and analyzed via AMS with 1-minute time resolution after Lee *et al.* (2011b), with the addition of (a) a continuously circulating water sheath around the reaction vessel for temperature control at ~22 C (AquaBox fish-tank pump, Model AA2005), (b) a water trap after the atomizer (intermittent visible water at the atomizer outlet, see supplement), and (c) a ^{210}Po neutralizer between the driers and the AMS (Fig. 1; Boris *et al.*, 2014). Photo-oxidations lasted between ~30–140 minutes; control experiments ran for ~20 minutes (see supplement). Photo-reactor and stir bar were cleaned with deionized water and air-dried between each experiment.

Five ambient cloud samples from Mt. Tai, China were used (named T1-4 and T7); T7 was oxidized with (T7PA) and without (T7) added pinonic acid (30 μM). See supplement section S3 and Shen (2011) for sampling, storage, and composition details. Generally, pinonic acid (PA) concentrations in cloud water are unknown; due to similarity between yields of pinonic acid (~0.1–1%), pinic acid (~1–5%), and pinonaldehyde (~0–1%) from α- and β-pinene aqueous oxidation (Yu *et al.*, 1999), we conjecture that ambient pinonic acid concentrations might be similar to those of pinic acid and pinonaldehyde (0.11 and 0.8 μM, respectively; van Pinxteren *et al.*, 2005). Species concentrations are normalized by total sulfate to correct noise from fluctuating atomizer output (supplement Sections S2 and S4 for detailed methodological assessment).

Hydroxyl radicals were produced via photolysis of hydrogen peroxide (300 μM). The resulting $[OH]_{aq}$ was quantified in the cloud samples (and deionized water for comparison purposes) via absorption spectroscopy of 202 nm light by salicylic acid, which was below detection limit in the cloud samples, preceded by reverse phase liquid chromatography separation to prevent measurement interference from other absorbing species (N = 3; accounting for salicylic acid direct photolysis and using the second-order rate constant of 1.6×10^{10} $M^{-1}s^{-1}$; see Boris *et al.*, 2014); these measurements yielded 1.9×10^{-14} M OH within the cloud water and $5.4 \pm 0.5 \times 10^{-14}$ M OH within pure water (Boris *et al.*, 2014).

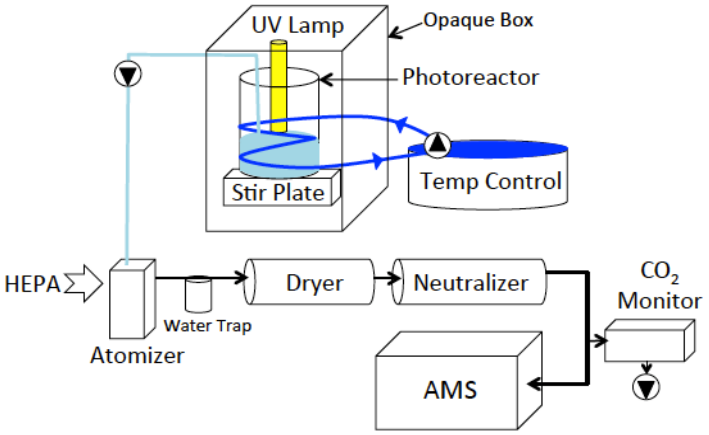

Fig. 1. Schematic of photoreactor experimental setup. Circles with black triangles indicate pumps.

Before hydrogen peroxide addition, these ambient cloud samples contained $[HOOH]_{aq}$ = 1–100 μM (Shen, 2011); assuming that the rate constant for OH production by hydrogen peroxide photolysis used herein holds in the complex ambient matrix, and that OH-organic reaction rate increases are linear within the given [OH] concentration range, this initial hydrogen peroxide content produces concentrations of $[OH]_{aq} \approx 10^{-15}$–$10^{-14}$ M which, adding the supplementary hydrogen peroxide, yields $[OH]_{aq} \approx 10^{-14}$ M. Ambient cloud [OH] is difficult to measure, but has been estimated at ~10^{-14} to 10^{-13} M (Jacob, 1986; Arakaki and Faust, 1998; Ervens *et al.*, 2003b; Deguillaume *et al.*, 2005; Ervens and Volkamer, 2010), 1–2 orders of magnitude lower than used in similar laboratory experiments (Lim *et al.*, 2010; Lee *et al.*, 2011a). These solutions are among the most atmospherically relevant used in the laboratory to date; methodological assessment of evaporative cycling effects and OH exposure is discussed further in supplement Section S4.

RESULTS

Control Experiments

Control experiments evaluated contributions of dark (noUV/noH_2O_2, 'baseline'), photolytic (+UV/noH_2O_2), and hydrogen peroxide-initiated (noUV/+H_2O_2) reactions to aqSOA. For ambient cloud samples from Mt. Tai, China (T1-T7), neither organic mass (Total Organics/Total Sulfate, normalized to t = 0) nor oxidation indicator *f*44 (mass at *m/z* 44/Total Organics, normalized to t = 0) change significantly under any of the control conditions, indicating probable dominance of OH-initiated reactions in the full photo-oxidations (Fig. S1).

Ambient Cloud Water Photo-Oxidation

Organic mass (Org/SO_4), O:C, and *f*44 (*m/z* 44/Org) for ambient cloud water photo-oxidation experiments are shown in Fig. 2; sample volume limited the duration of T1. Fig. 3 shows timelines of CO_2^+/SO_4 (Takegawa *et al.*, 2007), $C_2H_3O^+/SO_4$ (at *m/z* 43, indicating carbonyl content; McLafferty and Turecek, 1993), and $C_2H_3O^+/C_4H_7^+$ (ratio of most to least oxidized fragment at *m/z* 43), as well as $CH_2O_2^+/SO_4$, which is, nominally, formic acid (a major oxidation product of glyoxal compounds; see supplement S4 for caveats to formic acid quantification via AMS). Although determination of specific oxidative mechanisms is precluded by both fragmentation in the AMS and the complexity of the ambient cloud water composition, possible functionalization pathways are examined using delta analysis and movement in van Krevelen space.

Experiments may be grouped according to their oxidative behavior into two groups. In Functionalization-Dominant Regime 1 (T1 and T3) samples first gain, then lose organic mass, and gain, then sustain CO_2^+ fragments and *f*44 representing carboxylic acids (and other oxygenated fragments, as seen in difference spectra Fig. S4) indicating retention of oxygenated products. In contrast, in Fragmentation-Dominant Regime 2 (T4 and T7), organic mass is unchanging for the first 30–60 minutes and decreasing significantly thereafter; there is no increase in organic mass as seen in Regime 1. Additionally, there is early formation, then pronounced loss of oxygenated fragments; together, these suggest mass loss due to functional-group fragmentation. Evidence supporting these regime groupings is detailed in the following sections.

Functionalization-Dominant Regime 1: Oxygenated Products Maintained

For the T1 and T3 experiments with ambient Mt. Tai cloud water, Org/SO_4 increases for the first 15–30 minutes (to ~110% and ~140% of the t = 0 value, respectively), then decreases for the remainder of the experiment. Oxidation proxy *f*44 and carboxylic acid indicator CO_2^+/SO_4 increase for the first 15–30 minutes (T1 and T3); the T3 experiment ran longer and these proxies were observed to stay constant thereafter through 90 minutes. Reduction in $C_2H_3O^+/SO_4$ beginning at ~10 min may result from oxidation of carbonyls to carboxylic acids; contemporaneous rapid oxidation of C_xH_y species is indicated by an *increase* in $C_2H_3O^+/C_4H_7^+$ (from ~10–25 minutes in T1 and ~6–16 minutes in T3), indicating that $C_4H_7^+$ must be decreasing faster than $C_2H_3O^+$. After ~10–15 minutes, both $C_2H_3O^+/SO_4$ and $C_2H_3O^+/C_4H_7^+$ decrease, indicating a net loss of hydrocarbons and carbonyls. Most chemical change discernable via AMS occurs in the first half-hour or so of oxidation.

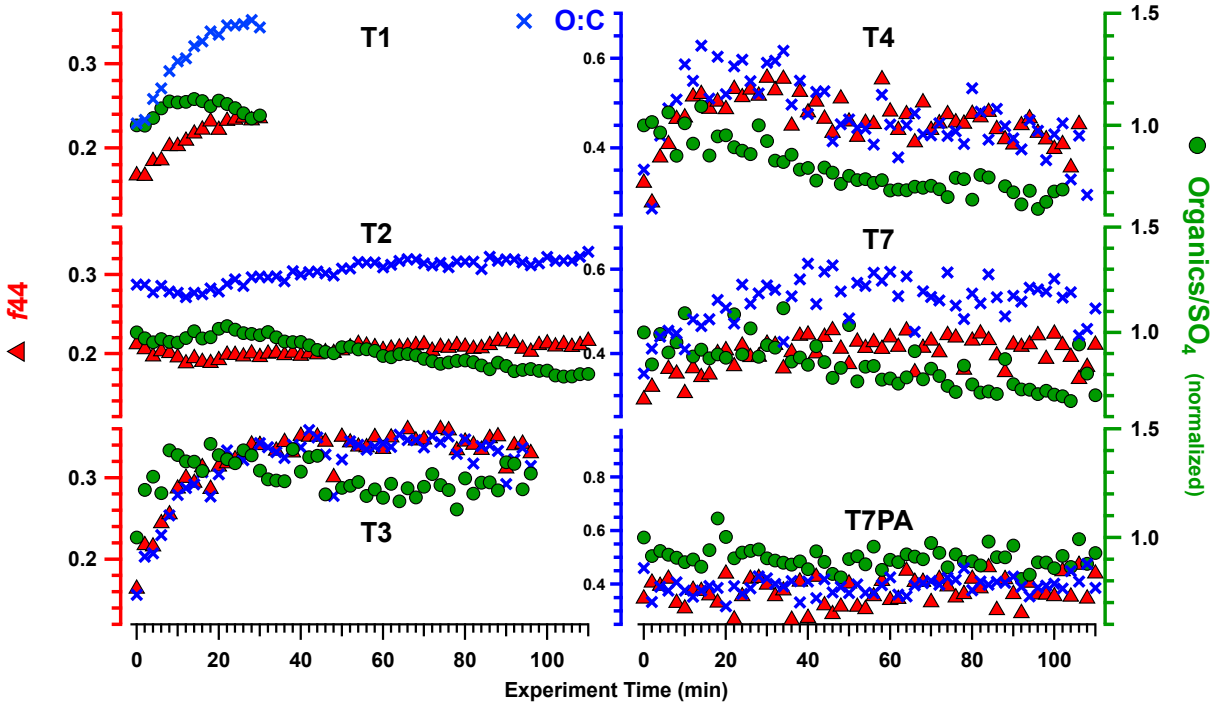

Fig. 2. Timelines of *f*44 (red), normalized (to t = 0) Org/SO_4 (green), and O:C (blue) for T1, T2, T3, T4-1, and T7 aqueous photo-oxidations. Uncertainties (not plotted): one standard deviation equals 28% of the value, from propagation of 20% AMS quantification error through the indicated calculations. Experiment time approximates ambient oxidation time as discussed in Section 2.3.

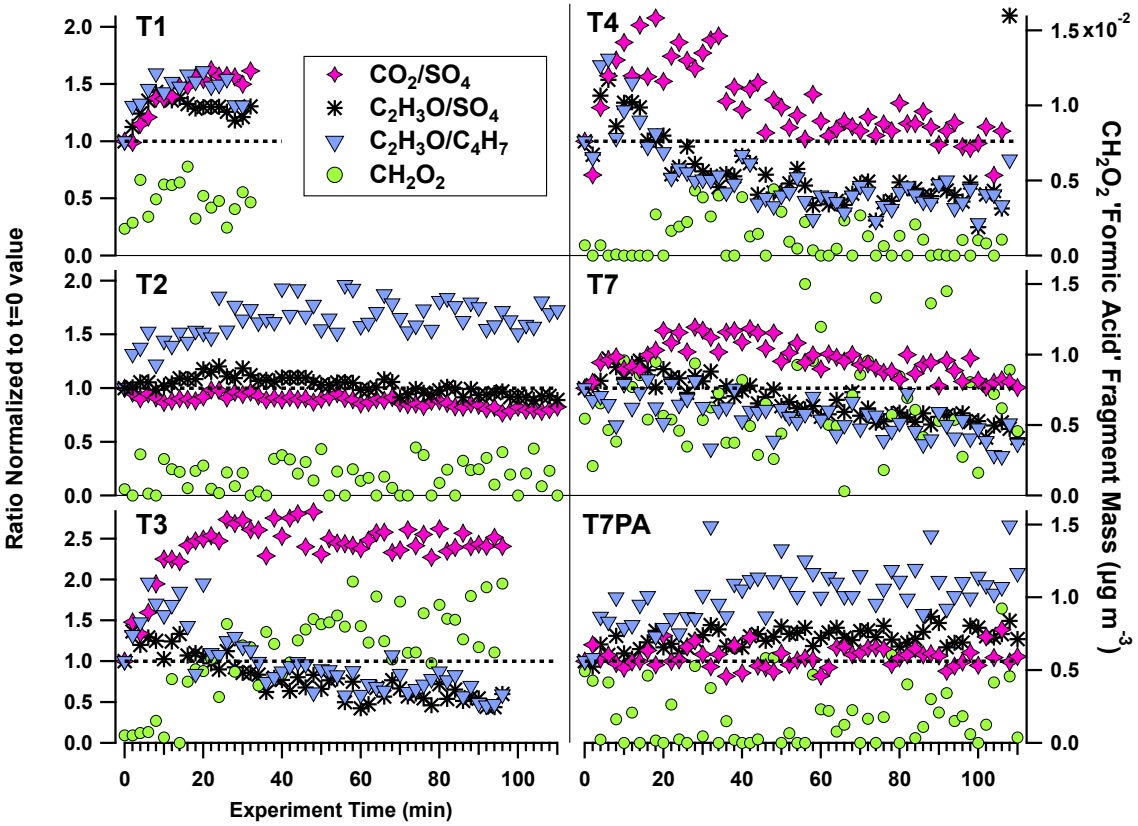

Fig. 3. Timelines of (left axes) fragment ratios normalized to the t = 0 value and (right axes) the mass concentration of the 'formic acid' fragment for T1-4, T7, and T7PA. Uncertainties (not plotted): one standard deviation equals 28% of the value, from propagation of 20% AMS quantification error through the indicated calculations.

A picture emerges of rapid oxidation of hydrocarbons to carbonyls and carbonyls to carboxylic acids, consistent with other similar studies (Lee *et al.*, 2011a). This is supported by difference spectra for the major organic fragment 'families' (CH, CHO, $CHO_{n>1}$; Fig. S4), in which CH fragments decrease and CHO and $CHO_{n>1}$ generally increase, especially at *m/z* 44 (CO_2^+); slight decreases in some CHO fragments commensurate with increases in $CHO_{n>1}$ fragments at the same *m/z* reflect oxidation of carbonyls to carboxylic acids. These patterns can also be seen in delta mass spectral analysis (see supplement S6 and discussion below).

The 'formic acid' fragment increases in both T1 and T3, suggesting that volatile formic acid and/or molecules fragmenting to $CH_2O_2^+$ are early-generation products. Formic acid production occurs in aqueous oxidations of glyoxal and is responsible for the eventual loss of total organic mass in those experiments due to its volatility and resultant loss during drying (Lee *et al.*, 2011b); the same mechanism could also be at play in T1 and T3, accompanied by decomposition of oxidized molecules to hydrocarbons and other non-formic-acid volatile fragments that are lost during evaporation as evidenced above.

Fragmentation may be further explored through the slope of movement in van Krevelen space (O:C vs. H:C, see Fig. 4) as an isolated particle/droplet population reacts (e.g., Heald *et al.*, 2010). T1 and T3, though with different compositions and therefore different starting positions in the diagram, move similarly toward enhanced O:C with slopes near –0.3, which is between m = –0.5, indicative of either carboxylic addition with C-C bond breakage or addition of both acid and alcohol/peroxide functional groups without fragmentation (total 1 H loss per 2 O addition, Fig. 4), and m = 0, indicative of alcohol or peroxide addition. Delta analysis can reveal which of these mechanisms are important (see supplement S6), as functional group composition dictates fragment *m/z* values such that delta (Δ) = *m/z* – 14*n* + 1, where *n* is the number of methylene (CH_2) bridges on the functional group (Table S3, McLafferty and Turecek, 1993). For T1 and T3, reductions in Δ_{-2}, Δ_0, and Δ_6, which may be partially attributed to alcohols (Table S3), suggests at least that alcohol addition does not exceed consumption of unsaturated hydrocarbons and carbonyls (at Δ_0, Δ_{-2}), and implies that carboxylic addition with C-C fragmentation is a more important reaction pathway for this dataset; this fragmentation may also contribute to the organic mass loss observed if the non-functionalized fragments are volatile. These slopes are similar to gas-phase chamber oxidations of both generated and ambient OA (Chhabra *et al.*, 2011; Lambe *et al.*, 2011; Ng *et al.*, 2011).

In contrast to experiments T1 and T3, there is relatively little change in composition during oxidation of T2. Org/SO_4 is unchanging for the first ~20 minutes, with subsequent decrease (Fig. 2). *f*44 increases slightly, but given that CO_2^+/SO_4 and $C_2H_3O^+/SO_4$ are constant (statistically, with a slight CO_2^+/SO_4 decrease toward the end), this is more a function of total organic mass loss than proportional gains at *m/z* 44; $C_2H_3O^+/C_4H_7^+$ increases in the first ~20 minutes, indicating decrease in hydrocarbon $C_4H_7^+$, which is echoed in general (though not universal) C_xH_y reduction in the difference mass spectrum (Fig. S4). However, clear progression toward higher O:C in the van Krevelen diagram (Fig. 4) implies that oxygenated compounds are gained; family difference spectra reveal increases in fragments > *m/z* 50 from the oxidized $CHO_{n>1}$ family, though fragment

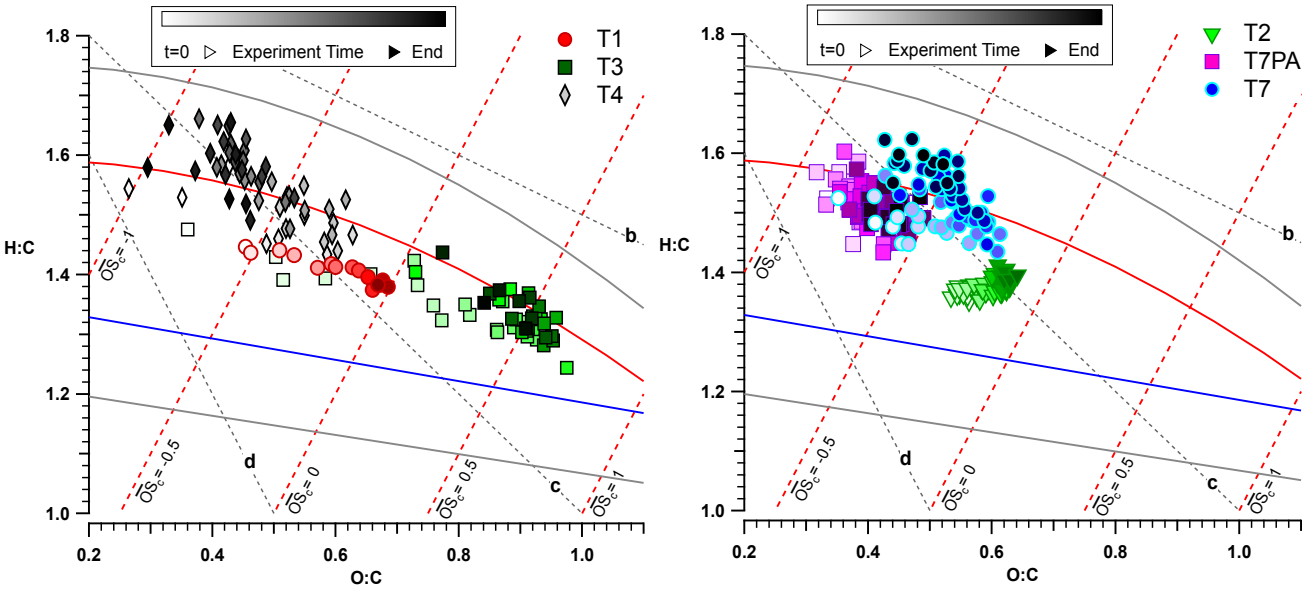

Fig. 4. van Krevelen diagram showing (left) T1, 3, and 4 full photo-oxidations and (right) T2, 7, and 7PA, colored by time during experiment. Dashed red lines: Estimated oxidation state, $OS_c = 2 \times O:C - H:C$ (Kroll *et al.*, 2011). Red and blue lines indicate the region usually inhabited by ambient data in the *f43* vs. *f44* plot, as transposed to van Krevelen space using the empirical parameterization of *f*43 vs. H:C and *f*44 vs. O:C for ambient and chamber OA (Ng *et al.*, 2010); grey lines represent 10% error. Linear fits: T1: m = –0.28, r^2 = 0.89; T2: m = 0.25, r^2 = 0.32; T3: m = –0.28, r^2 = 0.64; T4: m = –0.51 (see text), r^2 = 0.46; T7: m = –0.32 (see text), r^2 = 0.14; T7PA: m = –0.45, r^2 = 0.26.

abundance changes are small compared to the other experiments. The progression to highly oxidized ($CHO_{n>1}$) fragments > *m/z* 50 and decreased CO_2^+ suggests higher product stability against fragmentation within the AMS. By all measures, T2 started at a higher level of oxidation than the other experiments, which may reduce its ability to participate in further oxidation reactions, if, as discussed later, there exists a 'maximum' level of average solution oxidation above which subsequent organic mass formation is hindered.

Fragmentation-Dominant Regime 2: Oxygenated Fragments Lost

In Mt. Tai cloud water experiments T4 and T7, organic mass is unchanging for the first 30–60 minutes and decreasing significantly thereafter; there is no increase in organic mass. Fig. 2 shows that the normalized amount of Org/SO_4 does not increase as in Regime 1, but only decreases after the beginning of photooxidation at t = 0. There is some 'noise' in this data, which is discussed thoroughly in Supplement Section S2: *Description of variable atomizer output*; nonetheless, the normalized Org/SO_4 value begins to fall below 1 immediately after t = 0 and 'noise' does not exceed 1.09 in either T4 and T7, nor does it show the clear increasing, then decreasing trends seen in T1 and T3. This is in contrast to maximum normalized Org/SO_4 of 1.43 and 1.12 in T3 and T1.

O:C and *f*44 generally increase for the first 15–30 minutes and then decrease (Fig. 2). T4 and T7 show early formation, then pronounced loss (beginning at ~35–40 min) of CO_2^+/SO_4; the first half-hour looks similar to Regime 1 (T1 and T3), with fragment ratios indicating progressive carbonyl, then carboxylic acid increases (as above), but is followed by strong decreases in $C_2H_3O^+$ (to ~50% of t = 0 value in T4) and CO_2^+ (max ~200% at t = 20 min in T4; back to starting value by experiment's end). This is in clear contrast to Regime 1, in which oxygenated products were sustained throughout the experiments. The formic acid fragment is near zero in T4 and with some mass in T7, but shows no significant trend in either time series. The fragment-family difference spectra show universal hydrocarbon (CH) loss and decreased $C_2H_3O^+$ (*m/z* 43), with small increase or decrease in experiment-end CO_2^+ in T4 and T7, respectively, consistent with the fragment timelines.

In the van Krevelen diagram, T4 and T7 initially progress toward higher O:C and lower H:C as would be expected of the carbonyl and carboxylic acid formation inferred from the fragment ratios above, but then move back toward lower O:C and higher H:C as photo-oxidation progresses; along with the loss of organic mass and oxygenated fragments, this suggests that oxidized functional groups are chemically fragmented in solution and lost during atomization/drying, leaving behind the hydrocarbon 'backbones' of the molecules.

Ambient Cloud Water Photo-Oxidations with Added Pinonic Acid Precursor

In contrast to T7 and the other cloud samples, aqueous photo-oxidation of T7PA (T7 with added pinonic acid) has fairly constant Org/SO_4, *f*44, and CO_2^+/SO_4 (Figs. 2 and 3). $C_2H_3O^+/C_4H_7^+$ and moderate $C_2H_3O^+/SO_4$ increases imply hydrocarbon loss and carbonyl gains that are corroborated in the difference spectra (Figs. 3 and S4). In the van Krevelen diagram, T7PA resides in a region similar to T7 (Fig. 4); T7PA's lower starting O:C implies that unaltered T7 is on average even more functionalized than pinonic acid, which contains both a carboxylic acid and a carbonyl group. While T7PA develops slightly higher O:C and lower H:C with time (Fig. 4), these changes lack the amplitude and organization seen in T7 and the other samples in van Krevelen space. The family difference spectra reveal addition of CHO and $CHO_{n>1}$ fragments (including acids and carbonyls); delta analysis also indicates carbonyl formation in increasing Δ_2 (alkyls, saturated carbonyls).

T7PA differs from the unaltered sample (T7) in a number of ways. Addition of pinonic acid reduces the initial level of solution oxidation and pH, enhances formation of carbonyls and larger, more stable molecules (increased CHO and $CHO_{n>1}$ > *m/z* 50 fragments), and does not contain 'formic acid' signal; organic mass is maintained instead of decreased. This mass retention may be influenced by increasing total organic carbon (regardless of organic composition), as added PA constitutes a 57% increases in TOC for T7PA; increasing precursor concentration often results in higher mass production as hypothesized for this experiment and discussed in the introduction. Chamber pinonic acid-OH oxidations have resulted in highly functionalized, low-volatility molecules (Müller *et al.*, 2012) similar to unpublished pinonic acid aqueous photo-oxidations in our laboratory (identified via ESI-ToF-MS). Our observation of dominant carbonyl formation compares favorably to single-precursor pinonic acid photo-oxidations in our photoreactor (Schurman, 2014) and other aqueous *cis*-pinonic acid (Aljawhary *et al.*, 2016) and α-pinene oxidations (Bleier and Elrod, 2013); however, α-pinene products appear to vary with OH exposures, with dominant carboxylic acid formation and little change in *f*43 under high-OH conditions (George and Abbatt, 2010), and carbonyl formation in the form of acetone, formaldehyde, formic acid, etc. under lower [OH] (Nozière *et al.*, 1999); Lignell *et al.* (2013) show that direct aqueous PA photolysis is a minor mechanism. Since our precursor, pinonic acid, is a fairly early-generation α-pinene product and our equivalent OH exposure is approximately 1-to-1 with ambient exposure, our samples experience only a few hours of ageing compared to the days-to-weeks exposures in many chamber experiments that observe oxidation to carboxylic acids (which may be less relevant to cloud lifetimes, as well).

These results suggest that biogenic precursor addition may suppress or delay the oxidative mass loss of organics observed in aqueous photo-oxidations of unaltered cloud samples, and that total organic mass formation or loss may be related to the average level of solution oxidation. To investigate this, we evaluated the relationship between O:C, *f*44, and the incremental change in Org/SO_4, finding that mass decreases begin only when O:C > 0.61 ± 0.05, *f*44 > 0.23 ± 0.05 and, generally, *f*43 < ~0.08 ± 0.02 (T1 organic mass decreases occur with *f*43 steady at ~0.084, but this holds true for all other ambient-cloud experiments).

Because multiple fragments of different degrees of oxidation contribute to both *m/z* 43 and 44, the *f*44 and *f*43 'break-over points' (at which organic mass begins to decrease) may not be as useful (or universal) as that of O:C.

DISCUSSION

Two patterns emerge in these ambient cloud water photo-oxidations: in the first (Functionalization-Dominant Regime 1; T1 and T3), organic mass is gained, then lost, and sustained increases in highly oxidized fragments indicate overall organic acid formation; decrease in hydrocarbon fragments and production of the potentially-volatile $CH_2O_2^+$ fragment ('formic acid,' which partitions mostly to the gas phase; see discussion below and Liu *et al.*, 2012), suggests that volatilization of these species may contribute to mass decrease. In Fragmentation-Dominant Regime 2 experiments (T4 and T7), oxidized fragments decrease as mass decreases, indicating that oxidized functional groups are fragmented and lost to evaporation.

pH varies significantly between functionalization-dominant Regime 1 (pH ~5.5–6.4) and fragmentation-dominant Regime 2 (pH ~4.6–4.7; Fig. 5). These pH variations may drive formic acid production (or at least particle partitioning, as explained below), with substantial 'formic acid' fragments occurring only in samples with pH > ~5.5 (T1 and T3); T3 had the highest pH, and also the greatest increase in nominally formic acid fragments, while T1 had a lower pH and lower formic acid concentrations. In Regime 2, for which solution pH values were ≤ 4.74, little or no formic acid was detected. This is logical, since the Henry's Law partitioning of formic acid is driven toward the particle phase by higher pH (Liu *et al.*, 2012). Furthermore, particulate formic acid is enhanced significantly beyond the Henry's Law equilibrium in recent studies of urban-influenced particles (including one in Beijing, China; Wang *et al.*, 2007; Liu *et al.*, 2012); possible explanations include varying pH between particle bulk and surface (such that bulk measurements do not capture the pH relevant to the reaction) and variability in LWC (due to varying degrees of drying over the course of our experiments; Liu *et al.*, 2012). Also, cations such as Ca^{2+} can undergo acid-base reactions that lead to formic acid retention in the particle phase (Fornaro and Gutz, 2003; Löflund *et al.*, 2002; Malm *et al.*, 2009); this chemistry has been indirectly evidenced in one case, coincidently involving long-range transport of formic acid and dust from China (Kawamura *et al.*, 2012).

Initial solution O:C (ranging from 0.35–0.53) does not vary significantly between Regime 1 and Regime 2, but Regime 1 reactions generally end at higher O:C (0.69–0.95, versus ~0.64 for Type 2) due to retention of oxygenated functional groups. On average, Regime 1 samples had higher starting concentrations of TOC (Table 1), hydrogen peroxide, and other solutes, which may explain the tendency

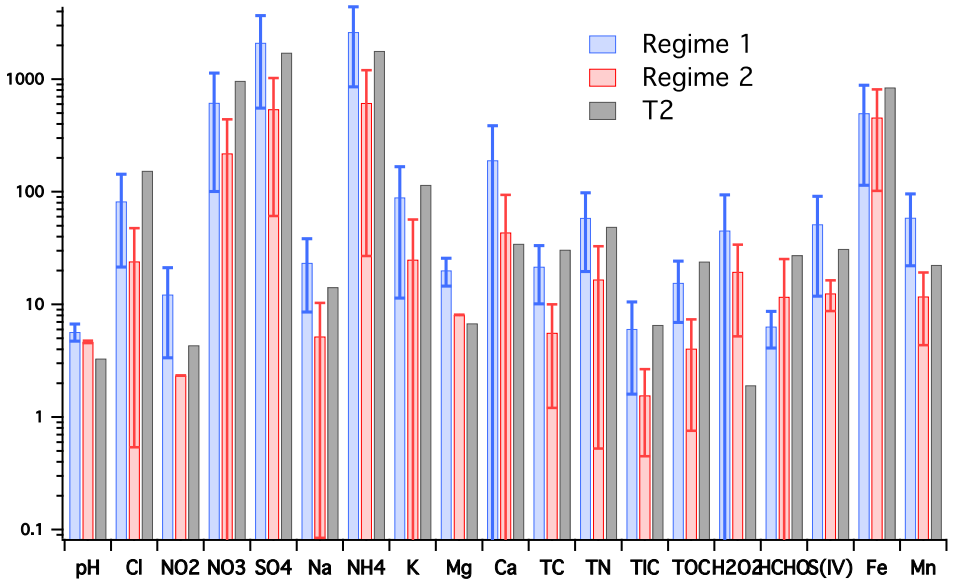

Fig. 5. Initial concentrations of the given cloud water constituents for given sample regimes. Units are, from left to right: Cl-Ca, HCHO, and S(IV) (μN); TC-TOC (ppm); Fe and Mn (μg L^{-1}). Error bars are standard deviations where data from multiple samples of the same regime were averaged. T2 consists of only one sample, so error bars are omitted.

Table 1. Initial total organic carbon (TOC, μg L^{-1}) in the given ambient cloud water sample (T#). *Due to low sample volume, T1 is a combination of three cloud samples; TOC and pH are estimated using averages of the three samples and assuming equal volumes.

	T1*	T2	T3	T4	T6PA	T7/7PA
TOC	~20	24.1	2.86	1.73	9.17	6.40/10.06
pH	~5.49	3.32	6.37	4.74	~3.7	4.58/~3.7

toward higher functionalization and therefore mass retention as described in the introduction; however, these concentration differences were not significant using the Mann-Whitney-Wilcoxon rank-sum test, and samples with equivalent TOC concentrations were found between the types (Fig. 5). Meteorological back-trajectories indicate the same source region (the heavily populated, industrial South China Plain) for air masses involved in all cloud samples (Shen, 2011).

Because it is difficult to both collect and to fully and continuously speciate cloud water, many studies use simple surrogate cloud water solutions to better constrain yields and reaction pathways, impeding direct comparison of our findings to the literature. However, using methods quite similar to those herein, though with higher OH concentrations, Lee *et al.* (2012) noted that ambient cloud samples formed highly oxidized SOA similar to that found in ambient aerosols, with organic mass production maxima of ~110–130% of the initial value followed by decreasing mass, similar to this work (Lee *et al.*, 2012). A model simulation of rural $SOA_{(aq+g)}$ with monoterpene emissions suggested ~21–25% SOA mass increase in the first ~1 hour when clouds (pH = 4.5) were added, with a slight reduction in mass after ~2 hours much like our experiments (Chen *et al.*, 2007a), while urban aerosol with anthropogenic emissions (NO_x, aromatics, alkanes) increased about 10% with no subsequent decrease; as in this work, model addition of less oxidized precursors appeared to augment and/or sustain aqSOA increases, supporting the hypothesis that pinonic acid addition would do the same. This hypothesis is also supported by a methacrolein cloud chamber photo-oxidation experiment involving a continuous interstitial source of less-oxidized precursors gases, which found a non-linear 47-fold increases in SOA mass sustained over a 22-hour experiment (Monod *et al.*, 2000, 2007; El Haddad *et al.*, 2009; Liu *et al.*, 2009).

The methodology used herein does differ from ambient cloud processing in some ways. First, bulk-phase photooxidations disregard the continuous evaporation and re-condensation of cloud droplets, which influences evaporative losses and the cycling of interstitial VOCs, semi-volatile compounds, oxidants, and oxygen (O_2) through the gas and droplet phases; this may in turn change aqSOA production (De Haan *et al.*, 2009). With typical cloud droplet lifetimes of ~10 minutes (Roelofs and Kamphuis, 2009), a real cloud could undergo 12 droplet cycles over the course of the experiments herein, implying a more continuous source of fresh interstitial VOCs than was recreated in our bulk-phase experiments. The bulk phase also limits gas exchange by eliminating droplet surface area at which exchange takes place: this lack of droplet surface area and attendant gas exchange may suppress both precursor absorption and volatile product evaporation (although drying before AMS analysis may offset the latter effect). The effect of evaporative cycling on aqSOA is a focus of current research.

In all, the bulk-aqueous/AMS analytical method is expected to lose a large and variable fraction of volatile oxidation products, the amount of which is highly dependent on the oxidation precursors and the volatility of their dominant products and is assumed to mimic the behavior of evaporating cloud droplets in the real atmosphere. Loss mechanisms may include a) evaporative loss during diffusion drying (Lee *et al.*, 2011a), and b) evaporative loss during drying as the particle beam enters the high vacuum in the AMS (Zelenyuk *et al.*, 2006). Mechanism a) might be more atmospherically relevant than b), but the current dataset cannot determine the contributions of each of these mechanisms to organic evaporative loss. Also, while the continuously-mixed bulk solution methodology might prevent the phase separation observed in atmospheric aerosol water (e.g., organic shells, which may change water evaporation and/or solute interaction and therefore reactivity), this effect is not thought to be important in cloud-relevant concentrations, where relative dilution leads to homogeneous mixing (Marcolli and Peter, 2005; Zuend *et al.*, 2008; Ziemann, 2010; Shiraiwa *et al.*, 2013). Under the assumption that the drying method used herein resemble those in the real atmosphere, the AMS does capture evaporated-cloud-relevant particulate organics.

CONCLUSIONS

This work explores how photooxidation influences ambient cloud water organic mass, oxidation state, and reaction regimes (such as functionalization versus fragmentation), and investigates relationships between oxidative progression and solution characteristics such as oxidation level (O:C) and initial total organic carbon (TOC). Unaltered ambient cloud water and 'biogenically influenced' ambient cloud water (via addition of pinonic acid) were photo-oxidized using UVC light and H_2O_2 (to form OH), atomized, and dried to simulate the formation of aqSOA from clouds; these experiments are among the first to quantify organic mass production in ambient cloud water and employ the most atmospherically relevant oxidant concentrations to date.

All ambient samples (except the heavily oxidized T2) gained carbonyl, then organic acid fragments; two of the five samples increased in sulfate-normalized organic mass (to a maximum of 110–140% of the t = 0 value). All samples eventually lost organic mass (reaching 60–80% of their initial values), which is attributed to formation of volatile products in some cases ('Functionalization-Dominant Regime 1' evidenced by increasing 'formic acid' fragment and sustained increases in CO_2^+) and molecular decomposition leading to loss of oxidized functional groups in others ('Fragmentation-Dominant Regime 2'; CO_2^+, $C_2H_3O^+$, O:C, and total organic mass decrease simultaneously); Regime 1 had significantly higher pH than Regime 2, and generally (though not significantly) higher initial total organic carbon, consistent with literature results showing formation of more functionalized products in higher-concentration solutions. The rate of aqSOA production in unaltered cloud water decreases as oxygenation increases, until organic mass loss beginning at a consistent value of O:C > 0.61 ± 0.05 and $f44 > 0.23 \pm 0.03$ ($f43 < 0.08 \pm 0.02$). This implies that there may be a parameterizable 'maximum oxidation level' for cloud water above which organic molecule fragmentation is dominant; however, we were unable to further

mathematically describe the relationship between aqSOA production/loss rate and oxidation level. The consistency of this 'maximum oxidation level' within the Mt. Tai cloud water should prompt further investigation of cloud samples with varying composition and concentration. If widely applicable, such a parameterization would contribute greatly to the understanding and modeling of the secondary organic aerosols that contribute to so many important health, environmental, and climate effects. Lastly, addition of TOC in the form of pinonic acid to an ambient sample (meant to simulate interstitial biogenic precursor absorption) appeared to prevent organic mass loss and foster carbonyl formation, rendering the un-altered experiments herein lower-bound estimations of aqSOA formation in photooxidized clouds.

ACKNOWLEDGMENTS

Collection of Mt. Tai cloud samples was funded by NSF Grant ATM-0711102. Thanks to Taehyoung Lee and Xinhua Shen for collecting the Mt. Tai cloud samples used in this study, and Tao Wang, Wenxing Wang, and Xinfeng Wang for their help and partnership in planning the Mt. Tai cloud sampling campaign.

SUPPLEMENTARY MATERIAL

Supplementary data associated with this article can be found in the online version at http://www.aaqr.org.

REFERENCES

Aljawhary, D., Zhao, R., Lee, A.K.Y., Wang, C. and Abbatt, J.P.D. (2016). Kinetics, mechanism, and secondary organic aerosol yield of aqueous phase photo-oxidation of α-Pinene oxidation products. *J. Phys. Chem. A* 120: 1395–1407.

Anastasio, C., Faust, B.C. and Allen, J.M. (1994). Aqueous phase photochemical formation of hydrogen peroxide in authentic cloud waters. *J. Geophys. Res.* 99: 8231–8248.

Arakaki, T. and Faust, B.C. (1998). Sources, sinks, and mechanisms of hydroxyl radical (•OH) photoproduction and consumption in authentic acidic continental cloud waters from Whiteface Mountain, New York: The role of the Fe(r) (r = II, III) photochemical cycle. *J. Geophys. Res.* 103: 3487–3504.

Atkinson, R. and Arey, J. (2003). Atmospheric degradation of volatile organic compounds. *Chem. Rev.* 103: 4605–4638.

Blando, J.D. and Turpin, B.J. (2000). Secondary organic aerosol formation in cloud and fog droplets: A literature evaluation of plausibility. *Atmos. Environ.* 34: 1623–1632.

Bleier, D.B. and Elrod, M.J. (2013). Kinetics and thermodynamics of atmospherically relevant aqueous phase reactions of α-pinene oxide. *J. Phys. Chem. A* 117: 4223–4232.

Boris, A.J., Desyaterik, Y. and Collett, J.L. (2014). How do components of real cloud water affect aqueous pyruvate oxidation? *Atmos. Res.* 143: 95–106.

Chang, J.L. and Thompson, J.E. (2010). Characterization of colored products formed during irradiation of aqueous solutions containing H_2O_2 and phenolic compounds. *Atmos. Environ.* 44: 541–551.

Chen, J., Griffin, R.J., Grini, A. and Tulet, P. (2007). Modeling secondary organic aerosol formation through cloud processing of organic compounds. *Atmos. Chem. Phys.* 7: 5343–5355.

Chhabra, P.S., Ng, N.L., Canagaratna, M.R., Corrigan, A.L., Russell, L.M., Worsnop, D.R., Flagan, R.C. and Seinfeld, J.H. (2011). Elemental composition and oxidation of chamber organic aerosol. *Atmos. Chem. Phys.* 11: 8827–8845.

Collett, J.L., Daube, B.C., Gunz, D. and Hoffmann, M.R. (1990). Intensive studies of Sierra Nevada cloudwater chemistry and its relationship to precursor aerosol and gas concentrations. *Atmos. Environ.* 24: 1741–1757.

De Haan, D.O., Corrigan, A.L., Tolbert, M.A., Jimenez, J.L., Wood, S.E. and Turley, J.J. (2009). Secondary organic aerosol formation by self-reactions of methylglyoxal and glyoxal in evaporating droplets. *Environ. Sci. Technol.* 43: 8184–8190.

Decarlo, P.F., Kimmel, J.R., Trimborn, A., Northway, M.J., Jayne, J.T., Aiken, A.C., Gonin, M., Fuhrer, K., Horvath, T., Docherty, K.S., Worsnop, D.R. and Jimenez, J.L. (2006). Field-deployable, high-resolution, time-of-flight aerosol mass spectrometer. *Anal. Chem.* 78: 8281–8289.

Deguillaume, L., Leriche, M. and Chaumerliac, N. (2005). Impact of radical versus non-radical pathway in the Fenton chemistry on the iron redox cycle in clouds. *Chemosphere* 60: 718–724.

El Haddad, I., Nieto-Gligorovski, L., Michaud, V., Temime-Roussel, B., Quivet, E., Marchand, N., Sellegri, K. and Monod, A. (2009). In-cloud processes of methacrolein under simulated conditions – Part 2: Formation of secondary organic aerosol. *Atmos. Chem. Phys.* 9: 5107–5117.

Ervens, B., George, C., Williams, J.E., Buxton, G.V., Salmon, G.A., Bydder, M., Wilkinson, F., Dentener, F., Mirabel, P., Wolke, R. and Herrmann, H. (2003a). CAPRAM 2.4 (MODAC mechanism): An extended and condensed tropospheric aqueous phase mechanism and its application. *J. Geophys. Res.* 108: 4426.

Ervens, B., Gligorovski, S. and Herrmann, H. (2003b). Temperature-dependent rate constants for hydroxyl radical reactions with organic compounds in aqueous solutions. *Phys. Chem. Chem. Phys.* 5: 1811–1824.

Ervens, B., Turpin, B.J. and Weber, R.J. (2011). Secondary organic aerosol formation in cloud droplets and aqueous particles (aqSOA): A review of laboratory, field and model studies. *Atmos. Chem. Phys.* 11: 11069–11102.

Ervens, B. and Volkamer, R. (2010). Glyoxal processing by aerosol multiphase chemistry: Towards a kinetic modeling framework of secondary organic aerosol formation in aqueous particles. *Atmos. Chem. Phys.* 10: 8219–8244.

Fischer, M. and Warneck, P. (1996). Photodecomposition of nitrite and undissociated nitrous acid in aqueous solution. *J. Phys. Chem.* 100: 18749–18756.

Fornaro, A. and Gutz, I.G.R. (2003). Wet deposition and related atmospheric chemistry in the São Paulo metropolis, Brazil: Part 2—Contribution of formic and acetic acids. *Atmos. Environ.* 37: 117–128.

Fu, T.M., Jacob, D.J., Wittrock, F., Burrows, J.P., Vrekoussis, M. and Henze, D.K. (2008). Global budgets of atmospheric glyoxal and methylglyoxal, and implications for formation of secondary organic aerosols. *J. Geophys. Res.* 113: D15303.

Galloway, M.M., Loza, C.L., Chhabra, P.S., Chan, A.W. H., Yee, L.D., Seinfeld, J.H. and Keutsch, F.N. (2011). Analysis of photochemical and dark glyoxal uptake: Implications for SOA formation. *Geophys. Res. Lett.* 38: L17811.

George, I.J. and Abbatt, J.P.D. (2010). Chemical evolution of secondary organic aerosol from OH-initiated heterogeneous oxidation. *Atmos. Chem. Phys.* 10: 5551–5563.

Graedel, T.E. and Weschler, C.J. (1981). Chemistry within aqueous atmospheric aerosols and raindrops. *Rev. Geophys.* 19: 505.

Graedel, T.E. and Goldberg, K.I. (1983). Kinetic studies of raindrop chemistry: 1. Inorganic and organic processes. *J. Geophys. Res.* 88: 10865.

Guzman, M.I., Colussi, A.J. and Hoffmann, M.R. (2006). Photoinduced oligomerization of aqueous pyruvic acid. *J. Phys. Chem. A* 110: 3619–3626.

Heald, C.L., Jacob, D.J., Park, R.J., Russell, L.M., Huebert, B.J., Seinfeld, J.H., Liao, H. and Weber, R.J. (2005). A large organic aerosol source in the free troposphere missing from current models. *Geophys. Res. Lett.* 32: L18809.

Heald, C.L., Kroll, J.H., Jimenez, J.L., Docherty, K.S., DeCarlo, P.F., Aiken, A.C., Chen, Q., Martin, S.T., Farmer, D.K. and Artaxo, P. (2010). A simplified description of the evolution of organic aerosol composition in the atmosphere. *Geophys. Res. Lett.* 37: L08803.

Herrmann, H., Hoffmann, D., Schaefer, T., Bräuer, P. and Tilgner, A. (2010). Tropospheric aqueous-phase free-radical chemistry: Radical sources, spectra, reaction kinetics and prediction tools. *Chemphyschem* 11: 3796–3822.

Jacob, D.J. (1986). Chemistry of OH in remote clouds and its role in the production of formic acid and peroxymonosulfate. *J. Geophys. Res.* 91: 9807.

Jang, M. (1999). Newly characterized products and composition of secondary aerosols from the reaction of α-pinene with ozone. *Atmos. Environ.* 33: 459–474.

Kanakidou, M., Seinfeld, J.H., Pandis, S.N., Barnes, I., Dentener, F.J., Facchini, M.C., Van Dingenen, R., Ervens, B., Nenes, A., Nielsen, C.J., Swietlicki, E., Putaud, J.P., Balkanski, Y., Fuzzi, S., Horth, J., Moortgat, G.K., Winterhalter, R., Myhre, C.E.L., Tsigaridis, K., Vignati, E., Stephanou, E.G. and Wilson, J. (2005). Organic aerosol and global climate modelling: A review. *Atmos. Chem. Phys.* 5: 1053–1123.

Kawamura, K., Imai, Y. and Barrie, L. (2005). Photochemical production and loss of organic acids in high Arctic aerosols during long-range transport and polar sunrise ozone depletion events. *Atmos. Environ.* 39: 599–614.

Kawamura, K., Matsumoto, K., Tachibana, E. and Aoki, K. (2012). Low molecular weight (C_1–C_{10}) monocarboxylic acids, dissolved organic carbon and major inorganic ions in alpine snow pit sequence from a high mountain site, central Japan. *Atmos. Environ.* 62: 272–280.

Kroll, J.H., Donahue, N.M., Jimenez, J.L., Kessler, S.H., Canagaratna, M.R., Wilson, K.R., Altieri, K.E., Mazzoleni, L.R., Wozniak, A.S., Bluhm, H., Mysak, E. R., Smith, J.D., Kolb, C.E. and Worsnop, D.R. (2011). Carbon oxidation state as a metric for describing the chemistry of atmospheric organic aerosol. *Nat. Chem.* 3: 133–139.

Lambe, A.T., Onasch, T.B., Massoli, P., Croasdale, D.R., Wright, J.P., Ahern, A.T., Williams, L.R., Worsnop, D.R., Brune, W.H. and Davidovits, P. (2011). Laboratory studies of the chemical composition and cloud condensation nuclei (CCN) activity of secondary organic aerosol (SOA) and oxidized primary organic aerosol (OPOA). *Atmos. Chem. Phys.* 11: 8913–8928.

Lee, A.K.Y., Herckes, P., Leaitch, W.R., Macdonald, A.M. and Abbatt, J.P.D. (2011a). Aqueous OH oxidation of ambient organic aerosol and cloud water organics: Formation of highly oxidized products. *Geophys. Res. Lett.* 38: L11805.

Lee, A.K.Y., Zhao, R., Gao, S.S. and Abbatt, J.P.D. (2011b). Aqueous-phase OH oxidation of glyoxal: Application of a novel analytical approach employing aerosol mass spectrometry and complementary off-line techniques. *J. Phys. Chem. A* 115: 10517–10526.

Lee, A.K.Y., Hayden, K.L., Herckes, P., Leaitch, W.R., Liggio, J., Macdonald, A.M. and Abbatt, J.P.D. (2012). Characterization of aerosol and cloud water at a mountain site during WACS 2010: Secondary organic aerosol formation through oxidative cloud processing. *Atmos. Chem. Phys.* 12: 7103–7116.

Lignell, H., Epstein, S.A., Marvin, M.R., Shemesh, D., Gerber, B. and Nizkorodov, S. (2013). Experimental and theoretical study of aqueous cis-pinonic acid photolysis. *J. Phys. Chem. A* 117: 12930–12945.

Lim, Y.B., Tan, Y., Perri, M.J., Seitzinger, S.P. and Turpin, B.J. (2010). Aqueous chemistry and its role in secondary organic aerosol (SOA) formation. *Atmos. Chem. Phys.* 10: 10521–10539.

Liu, J., Horowitz, L.W., Fan, S., Carlton, A.G. and Levy, H. (2012). Global in-cloud production of secondary organic aerosols: Implementation of a detailed chemical mechanism in the GFDL atmospheric model AM3. *J. Geophys. Res.* 117: D15303.

Liu, Y., El Haddad, I., Scarfogliero, M., Nieto-Gligorovski, L., Temime-Roussel, B., Quivet, E., Marchand, N., Picquet-Varrault, B. and Monod, A. (2009). In-cloud processes of methacrolein under simulated conditions – Part 1: Aqueous phase photooxidation. *Atmos. Chem. Phys.* 9: 5093–5105.

Loeffler, K.W., Koehler, C.A., Paul, N.M. and De Haan, D.O. (2006). Oligomer formation in evaporating aqueous glyoxal and methyl glyoxal solutions. *Environ. Sci.*

Technol. 40: 6318–6323.

Löflund, M., Kasper-Giebl, A., Schuster, B., Giebl, H., Hitzenberger, R. and Puxbaum, H. (2002). Formic, acetic, oxalic, malonic and succinic acid concentrations and their contribution to organic carbon in cloud water. *Atmos. Environ.* 36: 1553–1558.

Malm, W.C., Barna, M.G., Beem, K.B., Carrico, C.M., Collett, Jr., J.L., Day, D.E., Gebhart, K.A., Hand, J.L., Kreidenweis, S.M., Lee, T., Levin, E.J.T., McDade, C.E., McMeeking, G.R., Molenar, J.V., Raja, S., Rodriguez, M.A., Schichtel, B.A., Schwandner, F.M., Sullivan, A.P. and Taylor, C. (2009). *Rocky mountain atmospheric nitrogen and sulfur study*, Fort Collins, CO..

McLafferty, F.W. and Turecek, F. (1993). *Interpretation of mass spectra*, 4th ed., University Science Books, Herndon, VA.

Monod, A., Chebbi, A., Durand-Jolibois, R. and Carlier, P. (2000). Oxidation of methanol by hydroxyl radicals in aqueous solution under simulated cloud droplet conditions. *Atmos. Environ.* 34: 5283–5294.

Monod, A., Chevallier, E., Durandjoliboi, R., Doussin, J., Picquet-Varrault, B. and Carlier, P. (2007). Photooxidation of methylhydroperoxide and ethylhydroperoxide in the aqueous phase under simulated cloud droplet conditions. *Atmos. Environ.* 41: 2412–2426.

Müller, L., Reinnig, M.C., Naumann, K.H., Saathoff, H., Mentel, T.F., Donahue, N.M. and Hoffmann, T. (2012). Formation of 3-methyl-1,2,3-butanetricarboxylic acid via gas phase oxidation of pinonic acid – A mass spectrometric study of SOA aging. *Atmos. Chem. Phys.* 12: 1483–1496.

Ng, N.L., Canagaratna, M.R., Zhang, Q., Jimenez, J.L., Tian, J., Ulbrich, I.M., Kroll, J.H., Docherty, K.S., Chhabra, P.S., Bahreini, R., Murphy, S.M., Seinfeld, J.H., Hildebrandt, L., Donahue, N.M., DeCarlo, P.F., Lanz, V.A., Prévôt, A.S.H., Dinar, E., Rudich, Y. and Worsnop, D.R. (2010). Organic aerosol components observed in Northern Hemispheric datasets from Aerosol Mass Spectrometry. *Atmos. Chem. Phys.* 10: 4625–4641.

Ng, N.L., Canagaratna, M.R., Jimenez, J.L., Chhabra, P.S., Seinfeld, J.H. and Worsnop, D.R. (2011). Changes in organic aerosol composition with aging inferred from aerosol mass spectra. *Atmos. Chem. Phys.* 11: 6465–6474.

Nozière, B., Barnes, I. and Becker, K.H. (1999). Product study and mechanisms of the reactions of α-pinene and of pinonaldehyde with OH radicals. *J. Geophys. Res.* 104: 23645.

Oturan, M.A., Peiroten, J., Chartrin, P. and Acher, A.J. (2000). Complete destruction of *p*-nitrophenol in aqueous medium by electro-fenton method. *Environ. Sci. Technol.* 34: 3474–3479.

Schurman, M.I. (2014). *Characteristics, sources, and formation of organic aerosols in the Rocky Mountains*, Ph.D. thesis, Colorado State University, Fort Collins, Colorado, USA.

Shen, X. (2011). *Aqueous phase sulfate production in clouds at Mt. Tai in Eastern China*, Ph.D. thesis, Colorado State University, Fort Collins, Colorado, USA.

Takegawa, N., Miyakawa, T., Kawamura, K. and Kondo, Y. (2007). Contribution of selected dicarboxylic and omega-oxocarboxylic acids in ambient aerosol to the m/z 44 signal of an Aerodyne aerosol mass spectrometer. *Aerosol Sci. Technol.* 41: 418–437.

Tan, Y., Perri, M.J., Seitzinger, S.P. and Turpin, B.J. (2009). Effects of precursor concentration and acidic sulfate in aqueous glyoxal-OH radical oxidation and implications for secondary organic aerosol. *Environ. Sci. Technol.* 43: 8105–8112.

Tan, Y., Carlton, A.G., Seitzinger, S.P. and Turpin, B.J. (2010). SOA from methylglyoxal in clouds and wet aerosols: Measurement and prediction of key products. *Atmos. Environ.* 44: 5218–5226.

Tan, Y., Lim, Y.B., Altieri, K.E., Seitzinger, S.P. and Turpin, B.J. (2012). Mechanisms leading to oligomers and SOA through aqueous photooxidation: Insights from OH radical oxidation of acetic acid and methylglyoxal. *Atmos. Chem. Phys.* 12: 801–813.

Tsigaridis, K. and Kanakidou, M. (2003). Global modelling of secondary organic aerosol in the troposphere: A sensitivity analysis. *Atmos. Chem. Phys.* 3: 1849–1869.

Valverde-Canossa, J., Wieprecht, W., Acker, K. and Moortgat, G.K. (2005). H_2O_2 and organic peroxide measurements in an orographic cloud: The FEBUKO experiment. *Atmos. Environ.* 39: 4279–4290.

van Pinxteren, D., Plewka, A., Hofmann, D., Müller, K., Kramberger, H., Svrcina, B., Bächmann, K., Jaeschke, W., Mertes, S., Collett, J.L. and Herrmann, H. (2005). Schmücke hill cap cloud and valley stations aerosol characterisation during FEBUKO (II): Organic compounds. *Atmos. Environ.* 39: 4305–4320.

Volkamer, R.M., Ziemann, P.J. and Molina, M.J. (2009). Secondary Organic Aerosol Formation from Acetylene (C_2H_2): Seed effect on SOA yields due to organic photochemistry in the aerosol aqueous phase. *Atmos. Chem. Phys.* 9: 1907–1928.

Wang, Y., Zhuang, G., Chen, S., An, Z. and Zheng, A. (2007). Characteristics and sources of formic, acetic and oxalic acids in $PM_{2.5}$ and PM_{10} aerosols in Beijing, China. *Atmos. Res.* 84: 169–181.

Weschler, C.J., Mandich, M.L. and Graedel, T.E. (1986). Speciation, photosensitivity, and reactions of transition metal ions in atmospheric droplets. *J. Geophys. Res.* 91: 5189.

Yu, J., Cocker, D.R. III, Griffin, R.J., Flagan, R.C. and Seinfeld, J.H. (1999). Gas-phase ozone oxidation of monoterpenes: Gaseous and particulate products. *J. Atmos. Chem.* 34: 207–258.

Zellner, R., Exner, M. and Herrmann, H. (1990). Absolute OH quantum yields in the laser photolysis of nitrate, nitrite and dissolved H_2O_2 at 308 and 351 nm in the temperature range 278–353 K. *J. Atmos. Chem.* 10: 411–425.

Received for review, January 15, 2017
Revised, June 5, 2017
Accepted, June 5, 2017